Biophysical Journal
Article

Biophysical Society

Effect of H-Bond Donor Lipids on Phosphatidylinositol-3,4,5-Trisphosphate Ionization and Clustering

Zachary T. Graber,[1] Joseph Thomas,[2] Emily Johnson,[2] Arne Gericke,[3,*] and Edgar E. Kooijman[2]
[1]Department of Chemistry and [2]Department of Biological Sciences, Kent State University, Kent, Ohio; and [3]Department of Chemistry and Biochemistry, Worcester Polytechnic Institute, Worcester, Massachusetts

ABSTRACT The phosphoinositide, phosphatidylinositol-3,4,5-trisphosphate ($PI(3,4,5)P_3$), is a key signaling lipid in the inner leaflet of the cell plasma membrane, regulating diverse signaling pathways including cell growth and migration. In this study we investigate the impact of the hydrogen-bond donor lipids phosphatidylethanolamine (PE) and phosphatidylinositol (PI) on the charge and phase behavior of $PI(3,4,5)P_3$. PE and PI can interact with $PI(3,4,5)P_3$ through hydrogen-bond formation, leading to altered ionization behavior and charge distribution within the $PI(3,4,5)P_3$ headgroup. We quantify the altered $PI(3,4,5)P_3$ ionization behavior using a multistate ionization model to obtain micro-pK_a values for the ionization of each phosphate group. The presence of PE leads to a decrease in the pK_a values for the initial deprotonation of $PI(3,4,5)P_3$, which describes the removal of the first proton of the three protons remaining at the phosphomonoester groups at pH 4.0. The decrease in these micro-pK_a values thus leads to a higher charge at low pH. Additionally, the charge distribution changes lead to increased charge on the 3- and 5-phosphates. In the presence of PI, the final deprotonation of $PI(3,4,5)P_3$ is delayed, leading to a lower charge at high pH. This is due to a combination of hydrogen-bond formation between PI and $PI(3,4,5)P_3$, and increased surface charge due to the addition of the negatively charged PI. The interaction between PI and $PI(3,4,5)P_3$ leads to the formation of PI and $PI(3,4,5)P_3$-enriched domains within the membrane. These domains may have a critical impact on $PI(3,4,5)P_3$-signaling. We also reevaluate results for all phosphatidylinositol bisphosphates as well as for $PI(4,5)P_2$ in complex lipid mixtures with the multistate ionization model.

INTRODUCTION

Phosphoinositides (diacylphosphatidylinositolphosphates) are only minor constituents in cellular membranes; however, this class of lipids plays critical roles in a broad range of signaling events (1). Among the seven naturally occurring phosphoinositide species, phosphatidylinositol-3,4,5-trisphosphate ($PI(3,4,5)P_3$) exhibits the highest phosphorylation state and headgroup charge. Upon receptor stimulation, PI-3-kinase produces $PI(3,4,5)P_3$ from phosphatidylinositol-4,5-bisphosphate ($PI(4,5)P_2$), which leads to plasma membrane localization and activation of the Akt protein (2). The Akt protein is a key signaling protein that is involved in a range of cellular processes, including cell survival and proliferation (3). Although global $PI(3,4,5)P_3$ concentrations are very low, it has been shown that PI 3-kinase activation leads to the accumulation of the Akt protein in domains, suggesting that $PI(3,4,5)P_3$ is clustered (4–8). Because the Akt protein in these cases is colocalized with raft markers and/or the signaling event showed cholesterol dependence, it has been proposed that $PI(3,4,5)P_3$, which attracts the Akt protein to the plasma membrane, also enriches in lipid rafts. Although the inner leaflet composition and physical properties of lipid rafts are presently unknown, it is important to stress that the typical acyl chain composition of $PI(3,4,5)P_3$ is stearoyl-arachidonoyl, which is generally unfavorable for accumulation in a liquid-ordered lipid environment. It is noteworthy, however, that the presence of cholesterol promotes the formation of fluid phase phosphoinositide domains in ternary lipid mixtures (9). Although it remains to be seen how an outer leaflet liquid-ordered raft couples to an inner leaflet phosphoinositide-enriched domain and what phase state this inner leaflet domain adopts, it is

Submitted August 9, 2017, and accepted for publication October 13, 2017.

*Correspondence: agericke@wpi.edu

Zachary T. Graber and Joseph Thomas contributed equally to this work.

Zachary T. Graber's present address is Department of Chemistry, University of Pennsylvania, Philadelphia, Pennsylvania.

Joseph Thomas's present address is Department of Chemical and Biomolecular Engineering, New York University, Brooklyn, New York.

Editor: Francesca Marassi.

https://doi.org/10.1016/j.bpj.2017.10.029

striking that cholesterol is able to stabilize PI(3,4,5)P_3 domains. Outer leaflet liquid-ordered (raft) phases form because the hydrocarbon chains of a gel-phase-forming lipid, like sphingomyelin, interact with cholesterol, leading to increased mobility of the lipid's chains and a reduction of chain order. In contrast, formation of phosphoinositide domains is driven by interactions within the headgroup region. The clustering of phosphoinositides in the presence of bivalent cations, cationic peptides, or cationic patches of proteins is well documented (10–15). In a recent x-ray fluorescence study, we have shown that the interaction of PI(4,5)P_2 with Ca^{2+} is stronger than with Mg^{2+}, highlighting distinct structural requirements for the interaction of bivalent cations with the phosphoinositide headgroup (16). The unique structural properties of the phosphoinositide headgroup become even more apparent in the context of PIP clustering independent of bivalent cations or positively charged proteins/peptides. To explain the stabilization of phosphoinositide-enriched phases by cholesterol (13,17), we have proposed a model where cholesterol stabilizes a hydrogen-bond network that is being formed between the phosphoinositide headgroups (9,15,18). We have suggested that phosphoinositides dissipate the respective headgroup charge through a combination of intramolecular hydrogen-bond formation between the phosphomonoester group(s) and vicinal hydroxyl groups as well as intermolecular hydrogen-bond formation between neighboring PIP molecules (direct or water-mediated). In comparison to phosphatidic acid, where the negative charge is largely localized at the phosphomonoester group, diacylphosphatidylinositolphosphates are therefore able to smear out their charge, which leads to an intricate balance between charge-charge repulsive and attractive hydrogen-bond network forces. Although the insertion of cholesterol at first glance is expected to lead to increased spacing between the phosphoinositide molecules, monolayer experiments suggest that the opposite is actually happening, i.e., phosphoinositide molecules can pack more efficiently when cholesterol is present (9). Even though the cholesterol insertion results in some steric hindrance, the higher steric demand is apparently being compensated for by the participation of the cholesterol's hydroxyl group in the hydrogen-bond network formed between the phosphoinositide headgroups (9). Any chemical species present in the broader phosphoinositide headgroup region, be it another lipid with hydrogen-bonding capabilities, cholesterol, bivalent cations, or cationic peptides, will affect phosphoinositide domain formation. For example, we have shown that phosphatidylinositol promotes PI(4,5)P_2 domain formation as well (19). Whether or not phosphoinositide-enriched domains form will depend on the intricate balance between attractive and repulsive forces, which are governed by the nature and concentration of the chemical species present at the lipid/water interface. To summarize, whereas sphingolipid/cholesterol domains form in ternary mixtures with phosphatidylcholine (PC) due to a liquid-ordered/fluid demixing that is routed in interaction within the lipid chain moiety, phosphoinositide-enriched domains are fluid and form due to interactions within the headgroup region.

Interactions involving phosphoinositide headgroups, whether they are mutual phosphoinositide, phosphoinositide/lipid, or phosphoinositide/protein interactions, are strongly dependent on the ionization state of the phosphoinositide headgroup. In turn, the ionization state is strongly dependent on the physicochemical properties of the local environment (e.g., pH, concentration of bivalent cations) as well as the aforementioned interactions with other species. As these properties may vary in a highly dynamic fashion, the ionization state of the respective phosphoinositide may vary accordingly.

We have previously studied the ionization of PI(3,4,5)P_3 in multilamellar vesicles (MLVs) composed of the common zwitterionic lipid PC along with a small percentage of PI(3,4,5)P_3 (18). The ionization state of PI(3,4,5)P_3 was determined over the pH range from 4 to 11 using magic angle spinning (MAS) solid state ^{31}P NMR. PI(3,4,5)P_3 ionization was shown to follow a complex biphasic pattern, with the charge on the 4-phosphate first increasing before eventually decreasing as the 3- and 5-phosphates become deprotonated. Strikingly, the change toward slightly increased protonation of the 4-phosphate (even though the pH was raised) occurred near physiological pH. This surprising ionization behavior had been observed previously for inositol phosphates with three or more neighboring phosphate groups (20,21) and can be explained with the ability of the hydroxyl groups to stabilize negative charges at vicinal phosphate groups via hydrogen-bond formation. Because the 4-phosphate in PI(3,4,5)P_3 has no neighboring hydroxyl group (in contrast to the 3- and 5-phosphates), its charge cannot be stabilized via intramolecular hydrogen-bond formation to a hydroxyl group and as a consequence, it more strongly attracts the remaining proton. Our work thus highlighted that not only does the overall PIP charge change with pH, also the distribution of the charge within the headgroup varies with the pH value. In subsequent work we explored the ionization of PI(4,5)P_2 in the presence of the hydrogen-bond donor lipids PE and PI. These lipids not only influenced the charge of PI(4,5)P_2 via hydrogen-bond formation with the phosphomonoester groups, but in the case of PI, the lateral distribution of PI(4,5)P_2 was also altered, leading to the formation of macroscopic domains rich in PI and PI(4,5)P_2.

In this work, we examine the ionization of PI(3,4,5)P_3 in similarly complex membrane mixtures. Using, to our knowledge, a new quantitative model, we identified the impact of PE and PI lipids on the pH-dependent ionization behavior of PI(3,4,5)P_3. We find that these lipids interact with PI(3,4,5)P_3 in a manner similar to that of PI(4,5)P_2, resulting in altered charge and a change in the charge distribution on the PI(3,4,5)P_3 headgroup. Additionally, we observe the formation of macroscopic domains rich in PI and PI(3,4,5)P_3.

MATERIALS AND METHODS

Materials

1,2-dioleoyl-*sn*-glycero-3-phosphatidylcholine, 1,2-dioleoyl-*sn*-glycero-3-phosphatidylethanolamine, 1,2-dioleoyl-*sn*-glycero-3-phosphatidylinositol 3,4,5-trisphosphate (PI(3,4,5)P_3), L-α-phosphatidylinositol (liver, bovine), and 1,2-dioleoyl-*sn*-glycero-3-phosphoethanolamine-N-(lissamine rhodamine B sulfonyl) (ammonium salt) were purchased from Avanti Polar Lipids (Birmingham, AL). The acyl chain composition of liver PI is primarily stearoyl/arachidonoyl. Lipids were dissolved in a 2:1 by volume mixture of chloroform and methanol, except for the highly polar PI(3,4,5)P_3, which was dissolved in a 20:9:1 by volume mixture of chloroform/methanol/water. The concentrations of the gravimetrically prepared lipid stock solutions were verified by phosphate assay (according to Rouser et al. (22)). All stocks were observed running as a single spot on a TLC plate, indicating high purity.

NMR sample preparation

NMR samples were prepared from dry lipid films as described previously (23). Briefly, lipid stocks were mixed in appropriate volumes to form the desired lipid composition and evaporated in an inert N_2 atmosphere before drying overnight at 40–50°C in a high vacuum. Generally, 0.1 μmol of PI(3,4,5)P_3 was used in each sample and appropriate amounts of additional lipids were added to reach the desired lipid composition. Samples for a single titration curve were prepared at the same time to minimize variation between samples. Lipid films were hydrated with 2 mL of buffer containing 100 mM NaCl, 2 mM EDTA, and 50 mM buffering agent (20 mM citric acid, 30 mM MES for pH 4–6.5, 50 mM HEPES for pH 6.5–8.5, and 50 mM glycine for pH 8.5–11). Samples were vortexed thoroughly and freeze-thawed to form an MLV dispersion. The pH of each NMR sample was determined using an Intelli pH probe (Sentron, Roden, The Netherlands). The MLV dispersion was then spun-down for 45–60 min at 14,950–14,990 RPM (at 4°C) to create a lipid pellet, which was then loaded into a 4-mm zirconium MAS NMR sample tube for NMR analysis.

MAS NMR spectroscopy

MAS ^{31}P NMR spectra were recorded as previously described (23). A standard 85% H_3PO_4 solution was used as an external reference. NMR spectra were recorded under stable spinning conditions (5 kHz) at 21 $\pm$ 1.0°C. Static experiments were also used to confirm the predominance of the bilayer phase for each sample condition. Static spectra were acquired on the same probe using low-power proton decoupling (the spinal 64-pulse program was used for proton decoupling).

Preparation of giant unilamellar vesicles

Giant unilamellar vesicles (GUVs) were prepared using a modified electroformation protocol, as in Méléard et al. (24). An electroformation chamber was constructed using a 10-mm quartz cuvette with a Teflon top (Hellma Analytics, Müllheim, Germany). Holes were drilled in the top to allow the insertion of two parallel platinum wires (Sure Pure Chemetals, Florham Park, NJ). Wires were placed 9.6 mm apart from each other, then the ends of the wire above the Teflon cap were bent and wrapped in electrical tape to hold them in place. Wires had a diameter of 0.51 mm and a purity of 99.95%. Platinum was chosen for its high conductivity and resistance to corrosion. The parallel wires were evenly coated with a concentrated lipid solution prepared from a lipid film. Lipid films were prepared as previously described, then redissolved in 50 μL of 2:1 chloroform/methanol. The lipid mixture contained ~1 μmol of total lipid with 0.2 mol % Rhodamine-PE. The lipid mixture was spotted onto the wire in 2 μL aliquots, then allowed to dry under vacuum (−70 cm Hg) for 1 h. The cuvette was filled with an aqueous buffer containing 100 mM NaCl, 5 mM PIPES, 0.1 mM EDTA, and 100 mM sucrose (pH 7). The coated wires were submerged in the buffer and connected to a 2-channel waveform generator (Rigol Technologies, Beaverton, OR) via electric leads with alligator clips. Electroformation was performed in three steps over 2.5 h, with a slow increase in voltage followed by a swelling period and then a final step where frequency is slowly decreased (AC field parameters were used as in Méléard et al. (24)). Once formation of GUVs was complete, ~50 μL of the vesicle dispersion was transferred to each well of an eight well No. 1 borosilicate viewing plate (Nalge Nunc, Rochester, NY). An additional 150–200 μL of a dilution buffer was then added. This dilution buffer contained 100 mM NaCl, 5 mM PIPES, 0.1 mM EDTA, and 100 mM Glucose at pH 7. The addition of glucose results in a higher density on the interior of the GUVs (due to sucrose), leading to GUV sedimentation and facilitating GUV imaging.

Fluorescence microscopy

GUVs were observed using a model No. IX81 inverted epi-fluorescence microscope (Olympus, Tokyo, Japan) running SlideBook 6 software (3i, Enfield, CT). Images were viewed with a 40× long working distance lens (Olympus), and the lens jacket was adjusted accordingly to maximize resolution while focused. Images were taken with an Orca R2 digital charge-coupled device camera (Hamamatsu Photonics, Hamamatsu City, Japan). Exposure times ranged from 100–5000 ms, depending on fluorescence intensity and vesicle size. Images were processed using the software ImageJ (National Institutes of Health, Bethesda, MD). Vesicles were considered true GUVs if they only had one visible bilayer, were not significantly filled with other vesicles/lipids, and were not directly touching any other vesicles. Domain formation was observed as an area of altered local curvature (bulging) with moderate fluorophore exclusion.

Multistate fitting model

In Kooijman et al. (18), the ionization of many phosphoinositides was found to have an "inflection point" in the center of the curve, around pH 7. For PI(3,4,5)P_3 the effect is strikingly strong, with the 4-phosphate chemical shift actually decreasing over several pH units before increasing again (see Fig. 5 in Kooijman et al. (18)). Similarly complex ionization behavior was also observed for the corresponding inositol bisphosphates and trisphosphates (see the Supporting Material) (25,26). Although this biphasic behavior of the protonation state of the respective phosphate could be modeled simply with a two-pK_a Henderson-Hasselbach relation, this is an inaccurate representation, as each phosphate group actually undergoes only a single deprotonation event in the pH range 4–11, i.e., from −1 to −2 charge. To successfully model this behavior one must first understand the exact nature of the observed biphasic behavior. When two phosphate groups are adjacent, they can interact with each other through mutual hydrogen-bond formation, linking the deprotonation of the neighboring phosphate groups. Once one phosphate is deprotonated, this phosphate has a strong incentive to form hydrogen bonds to stabilize its charged state. In the case of adjacent phosphate groups, it can form a hydrogen bond with its protonated partner, and the resulting proton is then effectively shared between the two phosphates. This results in a more strongly attached proton after the first phosphate group is deprotonated. Thus, the phosphates are affected by the protonation state of the adjacent phosphate groups.

To describe this complex ionization, a separate pK_a (also referred to as "micro-pK_a") value is used to describe the deprotonation of a phosphate group when its partner(s) are protonated versus when they are deprotonated, in a similar manner to that described by Schlewer et al. (26) for the inositol polyphosphates. For PI(3,4,5)P_3, with its three phosphomonoester groups, there are eight distinct ionization states in the pH range of 4–11—one fully protonated state (three remaining protons), three singly deprotonated states, three doubly deprotonated states, and one fully deprotonated state. Each ionization state will relate to a separate pK_a to describe each deprotonation event. The model is illustrated in Fig. 1. To fit this theoretical model to the

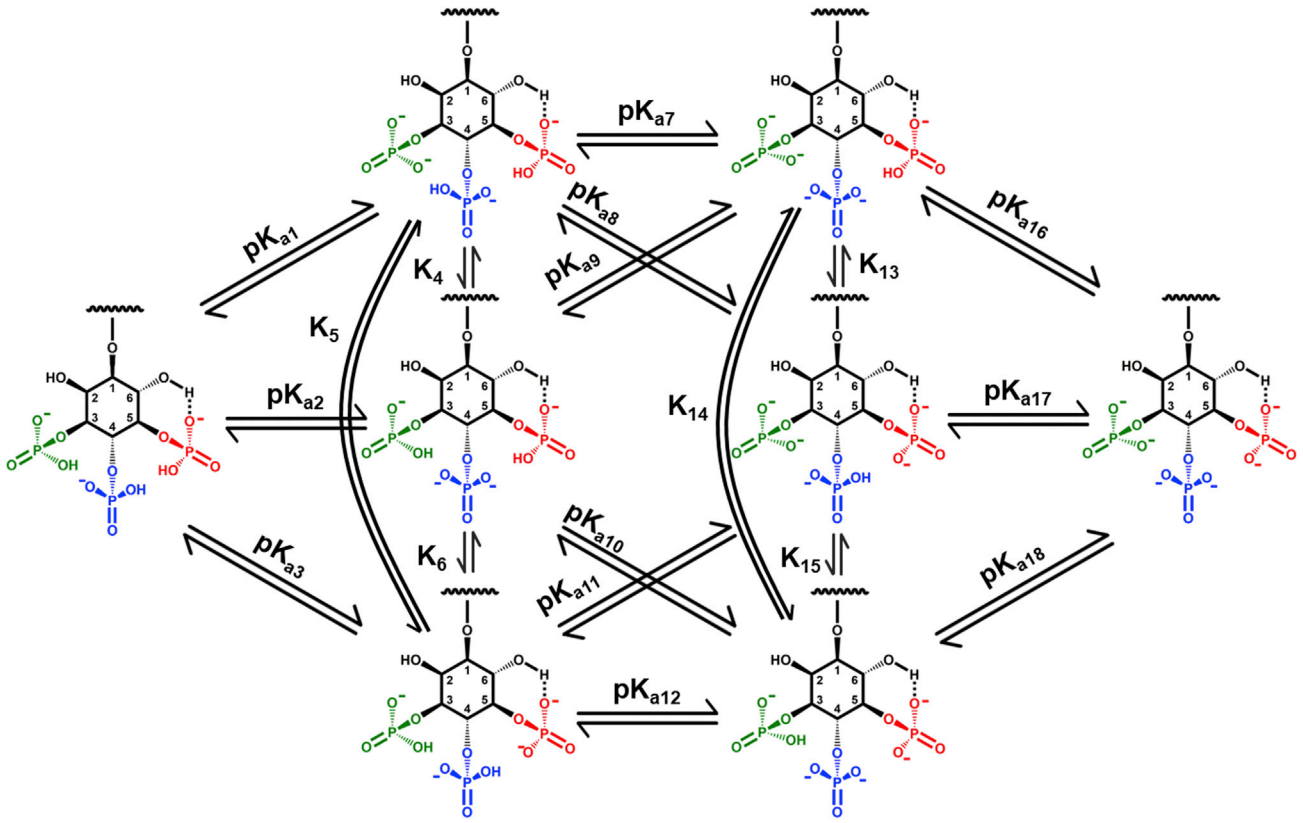

FIGURE 1 The ionization model for PI(3,4,5)P3$_3$. The model describes eight distinct states for the ionization of PI(3,4,5)P_3: the initial protonated state at pH 4 where each phosphate group carries one charge, three singly deprotonated states with the 3-, 4-, and 5-phosphate deprotonated, three doubly deprotonated states with the 3,4-, the 3,5-, and the 4,5-phosphates deprotonated, and the final state where all phosphates are fully deprotonated (at pH 11). pK$_{a1}$, pK$_{a2}$, and pK$_{a3}$ describe the deprotonation events from the protonated to singly deprotonated states. pK$_{a7}$, pK$_{a8}$, pK$_{a9}$, pK$_{a10}$, pK$_{a11}$, and pK$_{a12}$ describe the deprotonation events from the singly deprotonated states to the doubly deprotonated states. pK$_{a16}$, pK$_{a17}$, and pK$_{a18}$ describe the deprotonation events from the doubly deprotonated states to the fully deprotonated state. K_4, K_5, and K_6 describe the exchange between singly deprotonated states. K_{13}, K_{14}, and K_{15} describe the exchange between doubly deprotonated states. To see this figure in color, go online.

experimental data, the chemical shift of each phosphate group must be related to its current ionization state. The chemical shift of a single phosphate group at a specific pH can be represented as a weighted average of the chemical shifts of the protonated and deprotonated states, as follows (according to (27); additional details are given in the Supporting Material):

$$\delta = \frac{\delta_0[0] + \delta_3[3] + \delta_4[4] + \delta_5[5] + \delta_{34}[34] + \delta_{35}[35] + \delta_{45}[45] + \delta_{345}[345]}{[0] + [3] + [4] + [5] + [34] + [35] + [45] + [345]}, \quad (1)$$

where δ is the chemical shift at a specific pH, δ_X is the chemical shift of a given ionization state, and [X] is the concentration of an ionization state. Thus, each ionization state is attributed its own chemical shift and the chemical shift at a given pH is evaluated as a combination of the chemical shifts of each species present at that pH. For our model, we have eight separate ionization states, which must each be assigned its own chemical shift value. These chemical shift values are labeled according to the deprotonated phosphate in each ionization state (i.e., δ_0 is the fully protonated state, δ_{34} is the deprotonated 3- and 4-phosphate state). Here we make a basic assumption: the chemical shift for a given state will be primarily affected by the charge state of that phosphate, and will only be minimally affected by the charge state of any adjacent phosphate. Thus, for the 4-phosphate, we assume that all states with a protonated 4-phosphate (δ_0, δ_3, δ_5, and δ_{35}) will have a roughly equivalent chemical shift value, δ_{4p} (the chemical shift observed for the 4-phosphate at pH 4), whereas all states in which the 4-phosphate is deprotonated (δ_4, δ_{34}, δ_{45}, and δ_{345}), will be assumed to be equal to the observed chemical shift for the 4-phosphate when it is deprotonated (δ_{4d}; that is, the chemical shift observed for the 4-phosphate at pH $>$ 11). To determine the pK$_a$ values for each ionization step, we simply replace the concentrations in Eq. 1 based on the chemical equation for each equilibrium between the ionization states. Each chemical equation provides us with a relation between the concentration ratio and the pK$_a$. For pK$_{a1}$, this is represented as (see the Supporting Material for a complete description of each pK$_a$ relation):

$$\frac{[3]}{[0]} = 10^{\mathrm{pH}-\mathrm{pK}_{a1}}. \quad (2)$$

Now, by simply dividing the numerator and denominator by [0], we can substitute the concentration ratios to obtain an equation relating the chemical shift to the pK_a values describing the ionization behavior:

$$\delta = \frac{\begin{array}{c}\delta_0 + \delta_3 10^{(\mathrm{pH}-\mathrm{pK}_{a1})} + \delta_4 10^{(\mathrm{pH}-\mathrm{pK}_{a2})} + \delta_5 10^{(\mathrm{pH}-\mathrm{pK}_{a3})} \\ + \delta_{34} 10^{(2\mathrm{pH}-\mathrm{pK}_{a1}-\mathrm{pK}_{a7})} + \delta_{35} 10^{(2\mathrm{pH}-\mathrm{pK}_{a1}-\mathrm{pK}_{a8})} + \delta_{45} 10^{(2\mathrm{pH}-\mathrm{pK}_{a1}-\mathrm{pK}_{a10})} \\ + \delta_{345} 10^{(3\mathrm{pH}-\mathrm{pK}_{a1}-\mathrm{pK}_{a7}-\mathrm{pK}_{a16})}\end{array}}{\begin{array}{c}1 + 10^{(\mathrm{pH}-\mathrm{pK}_{a1})} + 10^{(\mathrm{pH}-\mathrm{pK}_{a2})} + 10^{(\mathrm{pH}-\mathrm{pK}_{a3})} \\ + 10^{(2\mathrm{pH}-\mathrm{pK}_{a1}-\mathrm{pK}_{a7})} + 10^{(2\mathrm{pH}-\mathrm{pK}_{a1}-\mathrm{pK}_{a8})} + 10^{(2\mathrm{pH}-\mathrm{pK}_{a1}-\mathrm{pK}_{a10})} \\ + 10^{(3\mathrm{pH}-\mathrm{pK}_{a1}-\mathrm{pK}_{a7}-\mathrm{pK}_{a16})}\end{array}}. \quad (3)$$

Equation 3 is used as the fit equation between our pH and chemical shift variables. Equation 3 has 15 unique parameters relating pH to chemical shift. Eleven of the pK_a values are not used in the equation and are calculated post-fit using the best parameters. Alternatively, Eq. 3 could also be rearranged to place these other pK_a values in the fitting equation. Either case results in equivalent pK_a values. A single fitting function is utilized to fit each of the phosphates. Each phosphate has different chemical shift values, resulting in a total of 15 fit parameters (seven pK_a values and eight chemical shift parameters for each phosphate). The chemical shift parameters are wrapped into six parameters—δ_{3p}, δ_{3d}, δ_{4p}, δ_{4d}, δ_{5p}, and δ_{5d}, representing the protonation state of each phosphate, e.g., for the 3-phosphate, δ_0, δ_4, δ_5, and δ_{45} were set to δ_{3p}. Nonlinear fitting was performed to minimize the sum of the χ^2-values from each data set. Peak chemical shift values for each data set were determined from MAS ^{31}P NMR spectra using the peak picking function of the software TopSpin (Bruker, Billerica, MA) and are accurate within ± 0.1 ppm. Uncertainty of the optimized fitting parameters was determined within one SD by examining the variance for each parameter that results in a one-unit variation in normalized χ^2. The initial values for the chemical shift parameters were set based on the minimum and maximum chemical shift values over their respective titration curve (representing the protonated and deprotonated chemical shift values, respectively) and held to ± 0.1 of their original values. Initial pK_a values were set to 6, 7, or 8, depending on whether it produces a singly deprotonated, doubly deprotonated, or fully deprotonated state. The pK_a values were allowed to vary between 3 and 10 to provide values consistent with the observed deprotonation of the phosphomonesters over that pH range (see Fig. 2).

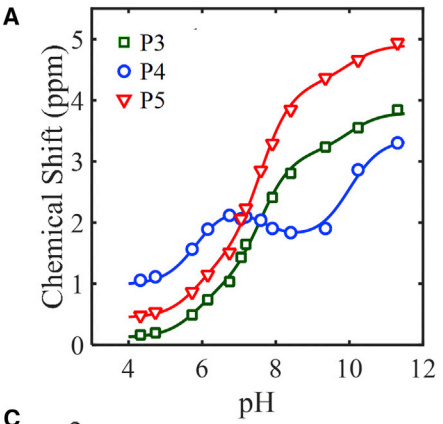

B

PC:PI(3,4,5)P_3			
pK_{a1}	6.48 ± 0.08	pK_{a10}	8.08 ± 0.06
pK_{a2}	6.10 ± 0.07	pK_{a11}	7.08 ± 0.1
pK_{a3}	6.52 ± 0.07	pK_{a12}	7.67 ± 0.1
K_4	2.42 ± 0.1	K_{13}	4.89 ± 0.1
K_5	0.93 ± 0.1	K_{14}	1.26 ± 0.2
K_6	0.38 ± 0.1	K_{15}	0.26 ± 0.2
pK_{a7}	7.80 ± 0.09	pK_{a16}	9.14 ± 0.1
pK_{a8}	7.11 ± 0.05	pK_{a17}	9.83 ± 0.1
pK_{a9}	8.19 ± 0.1	pK_{a18}	9.24 ± 0.2
Charge (at pH 7)			
P3	P4	P5	Pd
-1.33 ± 0.05	-1.48 ± 0.05	-1.33 ± 0.05	-1.00
Total	-5.14 ± 0.15		

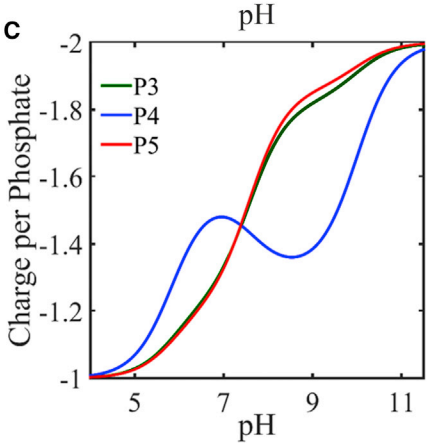

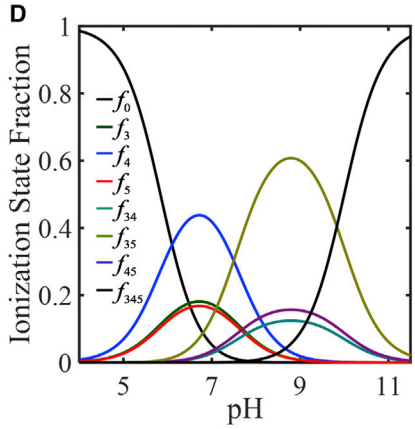

FIGURE 2 Fitting results for PI(3,4,5)P_3. (*A*) pH titration curve for PI(3,4,5)P_3 showing chemical shift versus pH. Data is from Kooijman et al. (18). Solid lines show the best fitting from the phosphatidylinositol trisphosphate fitting model. (*B*) Shown here is the table of pK_a values and charge at pH 7 based on the fit results. (*C*) Given here is a plot of the charge versus the pH for each phosphate. (*D*) Given here is a plot showing the relative prevalence of each ionization state. f_0 is the protonated fraction, f_3 is the fraction with P3 deprotonated, f_4 is the fraction with P4 deprotonated, f_5 is the fraction with P5 deprotonated, f_{34} is the fraction with P3 and P4 deprotonated, f_{35} is the fraction with P3 and P5 deprotonated, f_{45} is the fraction with P4 and P5 deprotonated, and f_{345} is the fully deprotonated fraction.

RESULTS AND DISCUSSION

Fitting of PI(3,4,5)P_3 ionization behavior

In our previous article, describing the ionization properties of PI(3,4,5)P_3, we used solid state ^{31}P NMR spectroscopy to determine the charge of PI(3,4,5)P_3 in MLVs composed of 95% PC and 5% PI(3,4,5)P_3 (note: here and throughout this article, % equals mol %) (18). The resulting ionization was described qualitatively, but we were unable to quantitatively model the complex ionization behavior. Using our newly developed model (see Materials and Methods) we are now able to provide a more detailed analysis of our previously published data for PI(3,4,5)P_3 (we also applied the model to all our previous PI(x,y)P_2 data; see the Supporting Material). This analysis will act as a comparison for the PI(3,4,5)P_3 ionization in complex lipid mixtures shown below. Fig. 2 *A* reproduces the PI(3,4,5)P_3 chemical shift data (from Kooijman et al. (18)) and the fitting curves that were calculated using the model shown in Fig. 1. The fitted pK_a values are shown in Fig. 2 *B*, whereas the charge and relative fractions of the ionization states are plotted in Fig. 2, *C* and *D*. Over the pH range 4–11, PI(3,4,5)P_3 has three sets of pK_a values, each corresponding to the removal of one proton (see Fig. 1). Starting at approximately pH 4, each of the three phosphomonoesters in the headgroup carries a single proton and one negative charge. The first proton comes off at roughly pH 6.5 (pK_{a1}, pK_{a2}, and pK_{a3}). The second proton pK_a lies between 7.1 and 8.2 (described by pK_{a7}, pK_{a8}, pK_{a9}, pK_{a10}, pK_{a11}, and pK_{a12}). The final deprotonation event has a pK_a of 9.1–9.8 (described by pK_{a16}, pK_{a17}, and pK_{a18}).

For the first deprotonation step, the 4-phosphate is deprotonated with greater probability than the other phosphates, as seen by the low pK_a of 6.10. The exchange constants (K_4, K_5, and K_6) show the preference for the deprotonated 4-phosphate: the transfer from deprotonated 3-phosphate to 4-phosphate has a constant of 2.4 (K_4), and the transfer from the 4-phosphate to 5-phosphate has a constant of 0.4 (K_6). The fraction of deprotonated 4-phosphate is more than twice the fraction of the other deprotonated phosphates (see Fig. 2 *D*). This can be understood by the position of the 4-phosphate in between the 3-, and 5-phosphate, and by its location in the headgroup-acyl chain interface. Although the orientation of the PI(3,4,5)P_3 headgroup in phospholipid bilayers has not been determined, we can deduce some information from the chemical shifts (CS) of the three phosphomonoesters. The CS of the 4-phosphate at this low pH (~6) is more deshielded than those of the 3-, and 5-phosphates, indicating a location closer to, or penetrating the aqueous environment outside of the lipid bilayer. This location (i.e., higher dielectric constant, see (28)) and the potential interactions (hydrogen bond, resonance stabilization, etc.) with the other two phosphates makes the 4-phosphate the preferred location for the first deprotonation event.

In the second deprotonation step, i.e., the removal of the next remaining proton, pK_{a8} and pK_{a11} are the lowest, both leading to the deprotonated 3- and 5-phosphates (f_{35}). The 3- and 5-phosphate-deprotonated state is more favored than the other ionization states, with exchange constants to the 3,5-deprotonated state of 4.9 (K_{13}) and 3.9 ($1/K_{15}$). The 3,5-phosphate deprotonated state is almost four times as prevalent as the other doubly deprotonated states (f_{35} versus f_{34} and f_{45}; see Fig. 2 *D*). The 3- and 5-phosphate-deprotonated state allows the charge to be spread out across the three phosphates, and is stabilized via hydrogen-bonding interactions with the 2-OH and the 6-OH. Thus, this deprotonation state is much more stable than the other double deprotonation states that involve the 4-phosphate (i.e., 3,4 or 4,5 positions deprotonated (f_{34} or f_{45})). This behavior is clearly seen in the titration curve (Fig. 2 *A*), where the 4-phosphate, instead of losing a proton receives a proton from either the 3-, or 5-phosphate, and thus becomes protonated again. This leads to the abnormal ionization behavior for the 4-phosphate of PI(3,4,5)P_3. The final deprotonation step requires a high pH value, as the fully deprotonated state carries a high charge density and a high negative surface potential leads to a significant lowering of the interfacial pH. Also, the 4-phosphate has no nearby hydrogen-bond donors to help stabilize its negative charge. From the stable 3,5-deprotonated state, the pK_a is as high as 9.8 (pK_{a17}).

At pH 7, as we find in cells, the overall charge (including the phosphodiester) is -5.14 ± 0.15. Although the total charge is higher than we have observed for phosphatidylinositol bisphosphates (which have charges ~−4 (see the Supporting Material)) (18), the individual charge on each phosphate group (P3, P4, and P5) is actually lower than for the respective phosphate groups in the phosphatidylinositol bisphosphates. This is not surprising, as the charge is reduced due to the proximity of multiple charged groups, and thus a higher surface charge density, leading to a lower interfacial pH. At pH 7, the deprotonated 4-phosphate is the most prominent form (f_4, see Fig. 2, *C* and *D*), although the 3,5-deprotonated state (f_{35}) increases rapidly from this point as the pH increases. The overall charge obtained with the more refined model presented here is similar to the charge obtained in our previous article using the simple two-step Henderson-Hasselbach formalism (−5.05) (18). However, here we find a higher charge on the 4-phosphate, leading to a slightly higher overall charge. Our quantitative model allows for a convenient evaluation of the charge state of each phosphomonoester in the headgroup of PI(3,4,5)P_3. With this new tool in hand, we set out to evaluate the effect of the hydrogen-bond donor lipids, PE, and PI, on the charge (distribution) of PI(3,4,5)P_3.

PI(3,4,5)P_3 ionization in the presence of PE

The ionization behavior of PI(3,4,5)P_3 is not static but varies depending on the bilayer environment. We have previously

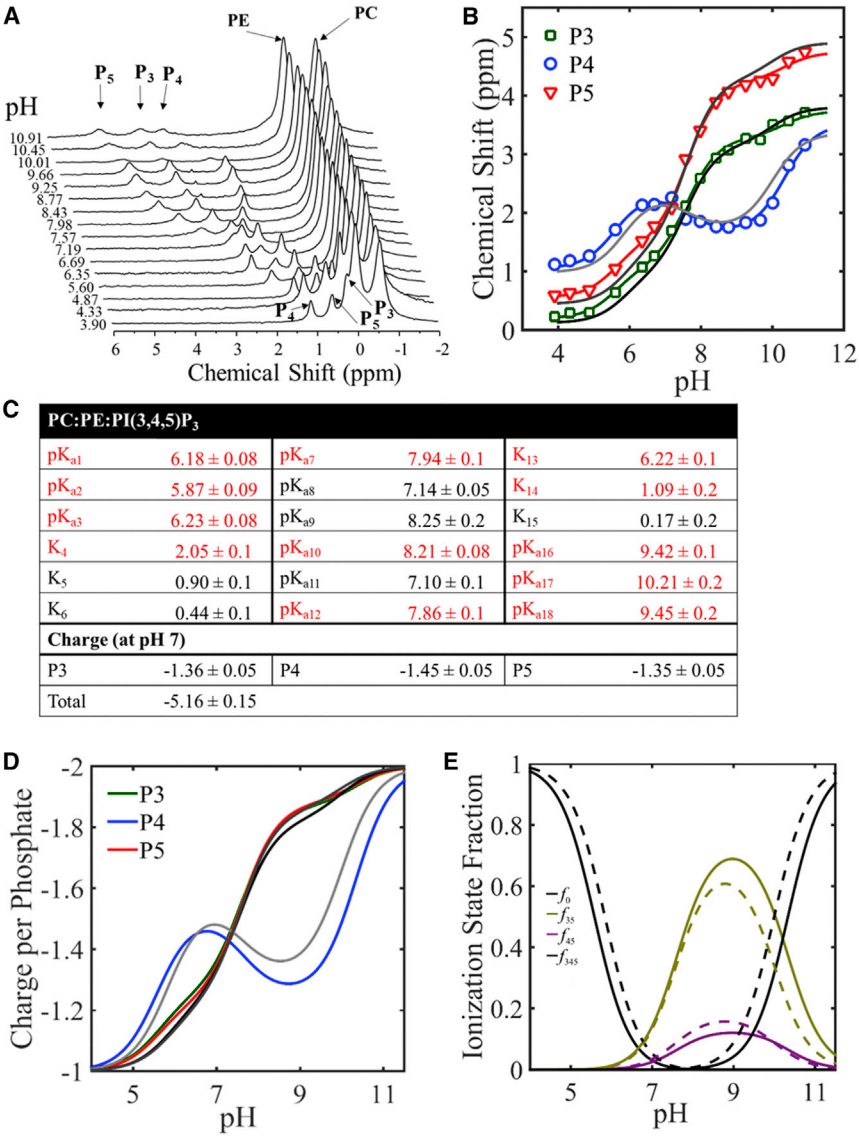

FIGURE 3 Ionization behavior of PI(3,4,5)P_3 in the presence of PE. (*A*) Shown here is the ^{31}P NMR data for 5 mol % PI(3,4,5)P_3 in 47.5 mol % PC, and 47.5 mol % PE. Chemical shift is relative to 85% H_3PO_4. (*B*) Given here is the pH titration curve showing the peak chemical shift versus pH. Solid lines show the best fitting from the phosphatidylinositol-trisphosphate fitting model. PC:PI(3,4,5)P_3 data (*gray lines*) are shown for comparison. (*C*) Shown here is a table of pK_a values and charge at pH 7 based on the fit results. pK_a values that changed relative to PI(3,4,5)P_3 in the absence of PE are marked in red. (*D*) Given here is a plot of the charge versus the pH for each phosphate. Charge values for PC:PI(3,4,5)P_3 data are shown in gray for comparison. (*E*) Given here is a plot showing the relative prevalence of each ionization state. For simplification purposes, only ionization states whose fractions changed significantly are shown. The PC:PI(3,4,5)P_3 ionization state fraction is shown as dashed lines for comparison. Fractions are labeled as above (see Fig. 2).

shown that the ionization of PI(4,5)P_2 can be significantly influenced by the presence of hydrogen-bond donor lipids in the membrane (19). Here we evaluate the impact of the hydrogen-bond donor lipid phosphatidylethanolamine (PE) on the ionization of PI(3,4,5)P_3. The impact of PE was investigated using MLVs composed of 47.5% PC, 47.5% PE, and 5% PI(3,4,5)P_3. NMR spectra were collected from samples with a range of pH values from 4 to 11 (Fig. 3 *A*). The chemical shift values obtained from the phosphate peaks are plotted in Fig. 3 *B*. The ionization follows a similar pattern as was observed in the absence of PE (Fig. 2 *A*), with the 4-phosphate initially acquiring the highest charge before lowering in charge as the other phosphates become deprotonated (Fig. 3 *D*). The presence of PE leads to a slight downfield shift of the phosphate group chemical shifts at low pH, as shown by the slight shift of the ionization curve to the left to lower pH values (see Fig. 3 *B*, and compare to PI(3,4,5)P_3 in the absence of PE (*gray curves*)). This shift to lower pH values indicates a higher charge at lower pH values as compared to PI(3,4,5)P_3 in the absence of PE. The increased charge is also reflected in the pK_a values derived from the chemical shift data, Fig. 3 *C*. The pK_a values that change in the presence of PE are marked in red in Fig. 3 *C*. In the presence of PE, the initial ionization step, i.e., the removal of the first of the last three remaining protons, is favored for each of the phosphates, with the pK_a values decreasing by ~0.27. The 3-phosphate deprotonation (pK_{a1}) drops from 6.48 to 6.18, the 4-phosphate deprotonation (pK_{a2}) drops from 6.10 to 5.87, and the 5-phosphate deprotonation (pK_{a3}) drops from 6.52 to 6.23, respectively. These decreased pK_a values suggest the formation of a hydrogen bond between PE and the PI(3,4,5)P_3 headgroup, leading to increased stabilization of the negative charge on each phosphate and therefore promoting deprotonation.

This is similar, but less in magnitude, to the effect we observed for PI(4,5)P_2 in the presence of PE ((19) and Fig. S5), where the pK_a values of the initial deprotonation events dropped by an average of 0.4. For PE, where there is just one phosphomonoester in the headgroup, this difference induced by PE was found to be almost one pH unit (see Table 1 in Kooijman et al. (27)). For PI(3,4,5)P_3, the additional intramolecular interactions between adjacent phosphates and hydroxyl groups leads to a stabilization of the deprotonated phosphomonoester state, and hence the effect of PE on the charge of each phosphate group is diminished.

As the PI(3,4,5)P_3 charge increases at higher pH values, the influence of the PE-PI(3,4,5)P_3 hydrogen-bond interaction on the PI(3,4,5)P_3 phosphate group ionization decreases. The pK_a values for the second ionization step, i.e., the removal of the second of the last two remaining protons, for the 4- and 5-phosphates are largely unaffected by the presence of PE. The pK_a values leading to a protonated P3 phosphate are slightly increased (pK_{a10} and pK_{a12} increase by an average of 0.16), suggesting an increased stabilization of the charged 3-phosphate. Indeed, as the pH increases above seven, the fraction of the 3- and 5-phosphate deprotonated state (f_{35}) and the charge on the 3- phosphate is increased in the presence of PE (see Fig. 3, *D* and *E*). Based on this, we conclude that PE interacts primarily with the 3- and 5-phosphates, with a slightly higher preference for the 3-phosphate. This is not surprising as the CS values for these phosphates are lower (more shielded) compared to that of the 4-phosphate. This indicates a position more deeply buried in the headgroup-acyl chain interface and thus the phosphate groups are more easily reachable by the primary amine of PE. In fact, the CS for the 3-phosphate is more shielded than that of the 5-phosphate, and we now find a slightly higher effect of PE on the charge of the 3-phosphate in accordance with a more deeply buried position.

The third ionization step leading to fully deprotonated PI(3,4,5)P_3 exhibits increased pK_a values in comparison to the PE free case, increasing by an average of 0.29 (pK_{a16}, pK_{a17}, and pK_{a18}). At these high pH values the amine group of PE itself starts to deprotonate, leading to an increased surface charge density and thus a lower interfacial pH (27). This lowering of the interfacial pH thus leads to the increased pK_a values we observe here for the final deprotonation of the PI(3,4,5)P_3 headgroup.

PI(3,4,5)P_3 ionization in the presence of PI

Phosphatidylinositol is an important phospholipid in the inner leaflet of the cell membrane, and acts as a precursor for the synthesis of phosphoinositides. The inositol ring of PI gives it many opportunities to interact with other lipids as a hydrogen-bond donor or acceptor. PI is also a negatively charged lipid, so the presence of PI will increase the negative surface charge density (higher negative surface potential) of the membrane, leading to a lower interfacial pH. Previously, we found a complex effect of PI on PI(4,5)P_2 ionization due to interaction between PI and PI(4,5)P_2 (19). The charge of PI(4,5)P_2 was unaffected for a pH between 4 and ~7. This unexpected behavior was rationalized by the fact that PI can serve as abundant hydrogen-bond donor and thus increase the charge of the 4-, and 5-phosphate, similar to the behavior described above for PE. However, the increased negative surface potential and the resulting lower pH value apparently results in a matching decrease of the negative charge of each phosphate, which yields an overall neutral effect on charge. The interaction between PI(4,5)P_2 and PI also led to the formation of PI and PI(4,5)P_2-rich clusters corroborating the ionization behavior.

Here we investigated the impact of PI on PI(3,4,5)P_3 ionization using vesicles composed of 88% PC, 10% PI, and 2% PI(3,4,5)P_3 (see Fig. 4 *A*). Chemical shift values are plotted in Fig. 4 *B* and the results from our fits are shown in Fig. 4, *C* and *D*. At low pH, the ionization curve is almost identical in the absence and presence of PI, similar to what we observed for PI(4,5)P_2. At higher pH, the curve shifts to the right, indicating increased protonation of the PI(3,4,5)P_3 phosphates. The pK_a values for the first ionization step, i.e., removal of the first of the last three remaining protons, are unchanged. However, whereas individual pK_a values are not largely changed at low pH, the exchange rates are significantly shifted (with K_4 decreasing and K_6 increasing; see Fig. 4 *C*), resulting in an increased fraction of deprotonated 3- and 5-phosphates as compared to the situation in the absence of PI (f_3 and f_5 increase; see Figs. 4 *E* and 2 *D*). At high pH, all pK_a values are increased, with pK_a values to the double deprotonated state increasing by an average of 0.44 ($pK_{a7–a12}$), whereas the pK_a values leading to the triple deprotonated state increase by an average of 0.55 (pK_{a16}, pK_{a17}, and pK_{a18}). The increased pK_a values result in a decreased total charge at higher pH compared to PI(3,4,5)P_3 in the absence of PI, −5.0 compared to −5.1.

The increased pK_a values at high pH ($pK_{a7–a18}$) can be explained by the increased negative surface potential in the presence of PI. At high pH the effect of the hydrogen-bond formation between the phosphates of PI(3,4,5)P_3 and the hydroxyl groups of PI is diminished, and the increase in negative surface charge density takes over. The negative surface potential attracts positively charged hydrogen ions to the interface, decreasing the interfacial pH value. The decreased pH leads to an increase in the apparent pK_a values as the increased proton concentration favors protonation of PI(3,4,5)P_3, identical to our previous observation of increased pK_a values at high pH for PI(4,5)P_2 in the presence of PI ((19) and Fig. S7). Although overall deprotonation is decreased, we still observe an increase in the doubly deprotonated 3- and 5-phosphate state (f_{35}) at high pH in the presence of PI, at the expense of the doubly deprotonated f_{34} and f_{45} states (see Fig. 4 *E*). This is comparable to the increase in the deprotonated 3- and 5-phosphates states

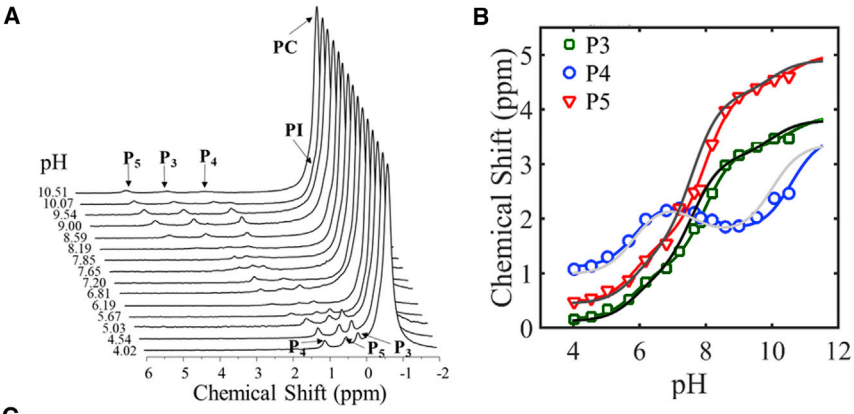

C

PC:PI:PI(3,4,5)P_3					
pK_{a1}	6.45 ± 0.09	pK_{a7}	8.27 ± 0.2	K_{13}	5.55 ± 0.2
pK_{a2}	6.15 ± 0.1	pK_{a8}	7.52 ± 0.07	K_{14}	1.16 ± 0.3
pK_{a3}	6.46 ± 0.09	pK_{a9}	8.57 ± 0.2	K_{15}	0.21 ± 0.2
K_4	1.99 ± 0.1	pK_{a10}	8.50 ± 0.1	pK_{a16}	9.69 ± 0.2
K_5	0.99 ± 0.1	pK_{a11}	7.52 ± 0.1	pK_{a17}	10.43 ± 0.3
K_6	0.50 ± 0.1	pK_{a12}	8.20 ± 0.2	pK_{a18}	9.75 ± 0.3
Charge (at pH 7)					
P3	-1.29 ± 0.05	P4	-1.45 ± 0.05	P5	-1.29 ± 0.05
Total	-5.03 ± 0.15				

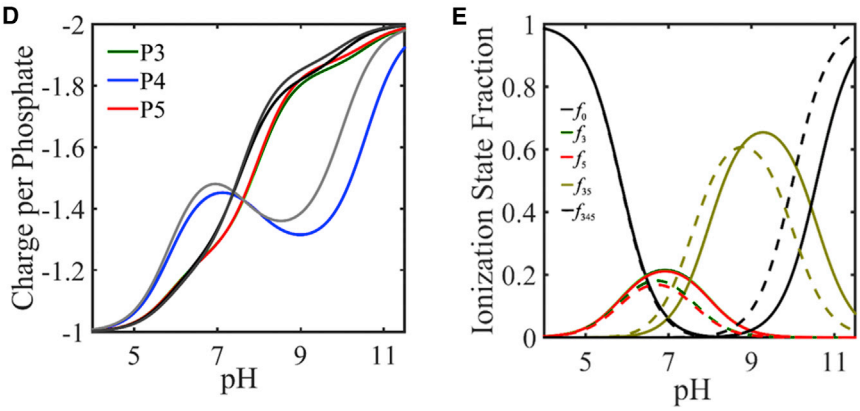

FIGURE 4 Ionization behavior of PI(3,4,5)P_3 in the presence of PI. (*A*) Shown here is the ^{31}P NMR data for 2 mol % PI(3,4,5)P_3 in 88 mol % PC, and 10 mol % PI. The chemical shift is relative to 85% H_3PO_4. (*B*) The pH titration curve shows the peak chemical shift versus pH. Solid lines show the best fitting from the phosphatidylinositol-trisphosphate fitting model. PC:PI(3,4,5)P_3 data (*gray lines*) are shown for comparison. (*C*) Given here is a table of pK_a values and charge at pH 7 based on the fit results. pK_a values that changed relative to PI(3,4,5)P_3 in the absence of PI are marked in red. (*D*) Given here is a plot of the charge versus the pH for each phosphate. Charge values for PC:PI(3,4,5)P_3 data are shown in gray for comparison. (*E*) Given here is a plot showing the relative prevalence of each ionization state. For simplification purposes, only those ionization states whose fractions changed significantly are shown. The PC:PI(3,4,5)P_3 ionization state fraction is shown as dashed lines for comparison. Fractions are labeled as above (see Fig. 2).

(f_3 and f_5) at low pH. The increased charge on the 3- and 5-phosphates in the presence of PI further suggests the presence of PI-PI(3,4,5)P_3 hydrogen bonds stabilizing the deprotonated 3- and 5-phosphates, even at high pH where the effect of the increased surface potential is dominant.

PI-dependent PI(3,4,5)P_3 cluster formation

The effect of PI on the ionization of PI(3,4,5)P_3 follows identical trends as those observed for PI(4,5)P_2. For PI and PI(4,5)P_2, we previously observed the formation of PI and PI(4,5)P_2-rich clusters. These domains are likely driven by the hydrogen-bond interactions between PI and PI(4,5)P_2, which result in spreading of the charge of the 4-, and 5-phosphate of PI(4,5)P_2 (19). Because our PI and PI(3,4,5)P_3 ionization data suggests the formation of similar hydrogen-bond interactions, it is reasonable to think that similar PI-PI(3,4,5)P_3-rich clusters may form as well. Given the large number of hydroxyl groups on the inositol ring that can act as hydrogen-bond donors or acceptors, it is likely that multiple hydrogen bonds could form between PI(3,4,5)P_3 and PI, resulting in a relatively strong interaction. To investigate if PI(3,4,5)P_3 clustering occurs in the presence of PI, we have examined GUVs containing PC, PI, and varying amounts of PI(3,4,5)P_3. All GUVs were formed under physiological buffer conditions to ensure that no artifacts occur due to abnormal salt conditions. Representative GUV images are shown in Fig. 5. Experiments were repeated at least twice, and very similar morphologies were observed in each case. In the absence of PI(3,4,5)P_3, the PC-PI vesicles show no domains, indicating that PC and PI do not normally phase-separate. When 5% PI(3,4,5)P_3 is included in the vesicle composition, the majority (>50%) of isolated, well-formed GUVs show the formation of a

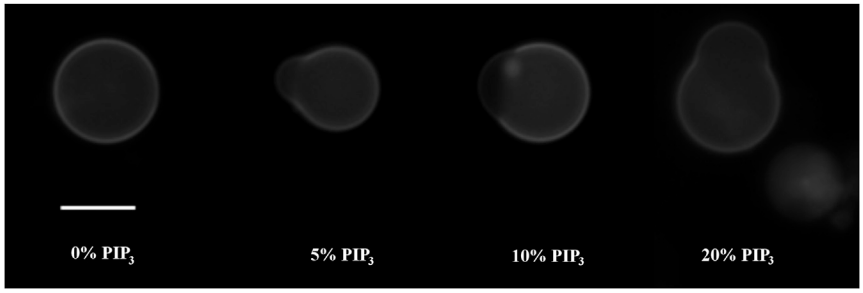

FIGURE 5 PI(3,4,5)P_3-rich clusters form in the presence of PI. GUVs were formed in physiological buffer conditions (100 mM NaCl, 5 mM PIPES, 0.1 mM EDTA, and 100 mM sucrose (pH 7)) with a lipid composition of 80-X%/20%/X% PC:PI:PI(3,4,5)P_3. GUVs were labeled by Rhodamine-B PE. GUV images are representative of the majority of GUVs in each mixture. In the presence of PI(3,4,5)P_3, a bulge-shaped domain is formed. Scale bar is 10 μm.

small bulge-shaped domain from which the rhodamine-PE fluorophore is partially excluded. As this bulge-shaped domain only forms in the presence of PI(3,4,5)P_3, it must be a result of PI(3,4,5)P_3 interacting with PI. This hypothesis is further strengthened by the observation that when the PI(3,4,5)P_3 content is increased, the domain size also increases proportionately. The additional PI(3,4,5)P_3 partitions into the bulge-shaped domain and the domain must therefore be PI(3,4,5)P_3-enriched.

PI-dependent clustering of PI(3,4,5)P_3 may have important implications for cellular signaling, creating locally increased concentrations of the normally rare PI(3,4,5)P_3. Given that PI(4,5)P_2 also exhibits PI-dependent clustering behavior, it is likely that PI(4,5)P_2 will also partition into these PI and PI(3,4,5)P_3-rich domains. We suggest that these phosphoinositide-rich clusters are likely to form in the cell plasma membrane, resulting in rich signaling platforms.

CONCLUSIONS

The ionization of the highly charged PI(3,4,5)P_3 plays an important role in interactions with signaling partners. The ionization of PI(3,4,5)P_3 is highly complex, with the 4-phosphate decreasing in charge around pH 7 as the 3- and 5-phosphate become more deprotonated. Slight shifts in the pH and chemical environment around PI(3,4,5)P_3 may lead to changes in the charge state of PI(3,4,5)P_3 and also the location of the charge on the PI(3,4,5)P_3 headgroup. The charge distribution is likely to affect the interaction of PI(3,4,5)P_3 with the binding pockets of its protein-partners. Especially considering the sensitivity of protein affinity to phosphomonoester charge (29,30). We have quantitatively modeled the ionization of PI(3,4,5)P_3 using a multistate ionization model. We found that hydrogen-bond donor lipids in the membrane interact with PI(3,4,5)P_3 and lead to subtle changes in the overall charge and charge localization (distribution) of the PI(3,4,5)P_3 headgroup. In the case of PE, we found a slight preference for interaction with the 3-phosphate, suggesting that the PI(3,4,5)P_3 headgroup orientation gives increased exposure to the 3-phosphate over the 5-phosphate for the primary amine of PE. The negatively charged phospholipid PI also interacts with PI(3,4,5)P_3 through hydrogen-bond formation. PI has a smaller impact on PI(3,4,5)P_3 charge as compared to PE, but the PI-PI(3,4,5)P_3 interaction leads to the formation of PI(3,4,5)P_3-rich clusters in the membrane. The PI-dependent cluster formation of both PI(3,4,5)P_3 and PI(4,5)P_2 (19) suggests that both of these phosphoinositides may exist as locally enriched clusters with PI in the inner leaflet of the plasma membrane. These phosphoinositide-rich clusters could act as signaling platforms at the membrane and may play an important role in mediating phosphoinositide-dependent signaling.

SUPPORTING MATERIAL

Supporting Materials and Methods and eight figures are available at http://www.biophysj.org/biophysj/supplemental/S0006-3495(17)31152-9.

AUTHOR CONTRIBUTIONS

Z.T.G., J.T., A.G., and E.E.K. designed the research. J.T. and E.J. performed experiments. Z.T.G. provided analytic tools and performed data analysis. Z.T.G., J.T., A.G., and E.E.K. wrote the manuscript.

ACKNOWLEDGMENTS

The authors thank Mona Mirheydari and Isaac Stokes for their assistance in preparing the giant unilamellar liposomes for the fluorescence microscopy experiments of PI-induced PI(3,4,5)P_3 domain formation.

We gratefully acknowledge support by the Chemistry Division of the National Science Foundation under grants CHE-1412920 and 1457873 (to E.E.K.), CHE-1058719 (to A.G. and E.E.K.), and CHE 1508499 (to A.G.).

SUPPORTING CITATIONS

Ref. (31) appears in the Supporting Material.

REFERENCES

1. Balla, T. 2013. Phosphoinositides: tiny lipids with giant impact on cell regulation. *Physiol. Rev.* 93:1019–1137.
2. Toker, A. 2012. Phosphoinositide 3-kinases—a historical perspective. *Subcell. Biochem.* 58:95–110.
3. Risso, G., M. Blaustein, …, A. Srebrow. 2015. Akt/PKB: one kinase, many modifications. *Biochem. J.* 468:203–214.

4. Lin, M. L., Y. C. Lu, …, S. S. Chen. 2014. Suppressing the formation of lipid raft-associated Rac1/PI3K/Akt signaling complexes by curcumin inhibits SDF-1α-induced invasion of human esophageal carcinoma cells. *Mol. Carcinog.* 53:360–379.
5. Gao, X., P. R. Lowry, …, J. Zhang. 2011. PI3K/Akt signaling requires spatial compartmentalization in plasma membrane microdomains. *Proc. Natl. Acad. Sci. USA.* 108:14509–14514.
6. Furt, F., S. König, …, S. Mongrand. 2010. Polyphosphoinositides are enriched in plant membrane rafts and form microdomains in the plasma membrane. *Plant Physiol.* 152:2173–2187.
7. Gao, X., and J. Zhang. 2008. Spatiotemporal analysis of differential Akt regulation in plasma membrane microdomains. *Mol. Biol. Cell.* 19:4366–4373.
8. Arcaro, A., M. Aubert, …, M. J. Seckl. 2007. Critical role for lipid raft-associated Src kinases in activation of PI3K-Akt signalling. *Cell. Signal.* 19:1081–1092.
9. Jiang, Z., R. E. Redfern, …, A. Gericke. 2014. Cholesterol stabilizes fluid phosphoinositide domains. *Chem. Phys. Lipids.* 182:52–61.
10. Wang, Y. H., D. R. Slochower, and P. A. Janmey. 2014. Counterion-mediated cluster formation by polyphosphoinositides. *Chem. Phys. Lipids.* 182:38–51.
11. Wang, Y. H., A. Collins, …, P. A. Janmey. 2012. Divalent cation-induced cluster formation by polyphosphoinositides in model membranes. *J. Am. Chem. Soc.* 134:3387–3395.
12. Ellenbroek, W. G., Y. H. Wang, …, A. J. Liu. 2011. Divalent cation-dependent formation of electrostatic PIP2 clusters in lipid monolayers. *Biophys. J.* 101:2178–2184.
13. Levental, I., D. A. Christian, …, P. A. Janmey. 2009. Calcium-dependent lateral organization in phosphatidylinositol 4,5-bisphosphate (PIP_2)- and cholesterol-containing monolayers. *Biochemistry.* 48:8241–8248.
14. McLaughlin, S., and D. Murray. 2005. Plasma membrane phosphoinositide organization by protein electrostatics. *Nature.* 438:605–611.
15. Graber, Z. T., A. Gericke, and E. E. Kooijman. 2014. Phosphatidylinositol-4,5-bisphosphate ionization in the presence of cholesterol, calcium or magnesium ions. *Chem. Phys. Lipids.* 182:62–72.
16. Graber, Z. T., W. Wang, …, E. E. Kooijman. 2015. Competitive cation binding to phosphatidylinositol-4,5-bisphosphate domains revealed by x-ray fluorescence. *RSC Adv.* 5:106536–106542.
17. Levental, I., F. J. Byfield, …, P. A. Janmey. 2009. Cholesterol-dependent phase separation in cell-derived giant plasma-membrane vesicles. *Biochem. J.* 424:163–167.
18. Kooijman, E. E., K. E. King, …, A. Gericke. 2009. Ionization properties of phosphatidylinositol polyphosphates in mixed model membranes. *Biochemistry.* 48:9360–9371.
19. Graber, Z. T., Z. Jiang, …, E. E. Kooijman. 2012. Phosphatidylinositol-4,5-bisphosphate ionization and domain formation in the presence of lipids with hydrogen bond donor capabilities. *Chem. Phys. Lipids.* 165:696–704.
20. Dozol, H., C. Blum-Held, …, B. Spiess. 2002. Inframolecular acid-base studies of the tris and tetrakis myo-inositol phosphates including the 1,2,3-trisphosphate motif. *J. Mol. Struct.* 643:171–181.
21. Guedat, P., G. Schlewer, …, B. Spiess. 1997. Investigation of the intramolecular acid-base properties of D-myo-inositol 1,3,4,5-tetrakisphosphate and DL-myo-inositol 1,2,4,5-tetrakisphosphate. *Chem. Commun.* 625–626.
22. Rouser, G., S. Fkeischer, and A. Yamamoto. 1970. Two dimensional then layer chromatographic separation of polar lipids and determination of phospholipids by phosphorus analysis of spots. *Lipids.* 5:494–496.
23. Graber, Z. T., and E. E. Kooijman. 2013. Ionization behavior of polyphosphoinositides determined via the preparation of pH titration curves using solid-state ^{31}P NMR. *Methods Mol. Biol.* 1009:129–142.
24. Méléard, P., L. A. Bagatolli, and T. Pott. 2009. Giant unilamellar vesicle electroformation from lipid mixtures to native membranes under physiological conditions. *Methods Enzymol.* 465:161–176.
25. Schmitt, L., P. Bortmann, …, B. Spiess. 1993. Myoinositol 1,4,5-triphosphate and related-compounds protonation sequence - potentiometric and P-31 NMR-studies. *J. Chem. Soc. Perkin Trans.* 2:2257–2263.
26. Schlewer, G., P. Guedat, …, B. Spiess. 1998. Inositol phosphates: inframolecular physico-chemical studies: correlation with binding properties. *In* Phosphoinositides: Chemistry. K. S. Bruzik, ed. American Chemical Society, Washington, DC, pp. 255–270.
27. Kooijman, E. E., K. M. Carter, …, B. de Kruijff. 2005. What makes the bioactive lipids phosphatidic acid and lysophosphatidic acid so special? *Biochemistry.* 44:17007–17015.
28. Strawn, L., A. Babb, …, E. E. Kooijman. 2012. The physical chemistry of the enigmatic phospholipid diacylglycerol pyrophosphate. *Front. Plant Sci.* 3:40.
29. Loew, S., E. E. Kooijman, and S. May. 2013. Increased pH-sensitivity of protein binding to lipid membranes through the electrostatic-hydrogen bond switch. *Chem. Phys. Lipids.* 169:9–18.
30. Young, B. P., J. J. Shin, …, C. J. Loewen. 2010. Phosphatidic acid is a pH biosensor that links membrane biogenesis to metabolism. *Science.* 329:1085–1088.
31. Slochower, D. R., P. J. Huwe, …, P. A. Janmey. 2013. Quantum and all-atom molecular dynamics simulations of protonation and divalent ion binding to phosphatidylinositol 4,5-bisphosphate (PIP_2). *J. Phys. Chem. B.* 117:8322–8329.